Journal of Undergraduate Chemistry Research, **2025**, 24 (4), 96

MOLECULAR PROPERTIES OF $[Ag_{20}\text{-}C_{60}\text{-}Ag_{20}]^{n-}$ SILVER-C_{60}-SILVER INTERFACE: A THEORETICAL INVESTIGATION

Tecarla S. Ikard* and Jairo Castillo-Chará†

Department of Chemistry, Physics & Materials Science, Fayetteville State University, Fayetteville, NC 28301

Abstract

In this work, molecular geometries, HOMO-LUMO gaps, Fermi levels, and Mulliken charges were calculated for the σ-bent, σ-linearly and π-linearly bonded $[Ag_{20}\text{-}C_{60}\text{-}Ag_{20}]^{n-}$ (n=0-3) complexes using the density functional B3LYP method and the LANL2DZ basis sets. With the Ag-C bond distances of 2.36 and 3.05 Å, respectively, the global minimum structure is the σ-bent $\eta^{1(b)}\text{-}[Ag_{20}\text{-}C_{60}\text{-}Ag_{20}]^{2-}$ complex. The calculated Mulliken charges suggest that the electrostatic interaction between the Ag_{20} clusters and the C_{60} molecule plays a significant role in the electron-conducting properties and stability of the $[Ag_{20}\text{-}C_{60}\text{-}Ag_{20}]^{n-}$ (n=0-3) complexes. The HOMO-LUMO gaps of the $[Ag_{20}\text{-}C_{60}\text{-}Ag_{20}]^{-n}$ complexes were found consistently lower than that of the C_{60} molecule, as well as those of the $[Au_{20}\text{-}C_{60}\text{-}Au_{20}]^{-n}$ complexes (4). The Fermi levels calculations indicate that the zero-charged singlet $[Ag_{20}\text{-}C_{60}\text{-}Ag_{20}]$ complexes with Fermi levels 1 eV above -5.36 eV, the Fermi level of the free C_{60} molecule, are the most suitable for electron conduction through the $Ag_{20}\text{-}C_{60}\text{-}Ag_{20}$ interface.

†Corresponding author: jcastill@uncfsu.edu *Undergraduate researcher and co-author
Keywords: HOMO-LUMO; Fermi-levels; $Ag_{20}\text{-}C_{60}\text{-}Ag_{20}$; Orbital Interactions; B3LYP; LANL2DZ.
Received: August 6, 2025 Accepted: September 5, 2025 Revision Received: September 15, 2025 Published: September 17, 2025

Introduction

The electron population distribution of metal-organic molecule-metal nanodevices is quite different from bulk materials and single molecules. Therefore, the study of their structure and conductive properties needs to be conducted extensible and reliable[1-3]. The metal-C_{60}-metal interface can be modeled as a nanocontact, which will be important in the performance of electronic nanodevices[3]. The electronic structure at the electrode surface is not well understood, however high degree of roughness is expected[1]. The electrode roughness can be modeled using metallic clusters of diverse sizes[1-3]. This is one approach that theoretical chemists and scientists working in molecular electronics and related fields are currently using to model electron transport properties of prototype complexes to mimic electron transport across the metal-C_{60}-metal interface[1-4]. Recent theoretical investigations in the $[Au_{20}\text{-}C_{60}\text{-}Au_{20}]^{n-}$ (where n = 0-3) molecular structures[1,4], suggest that gold clusters form stronger complexes with the C_{60} molecule than silver does, and with delocalized Fermi levels and potential applications for electron conduction within the metal-C_{60}-metal interface[5].

In the last two decades, electron transport studies at the nano-scale regime have developed significantly and promise to be an area of development for amazingly futuristic technological applications [6,7,8]. Recent measurements have definitively shown that the coupling of the C_{60} molecule oscillation frequency interacting with a gold surface results in single-electron transfer processes on the gold surface[5]. Electron conduction of fullerenes is determined by the fullerene bonding geometries on the metal electrodes[9]. The coupling and alignment of the C_{60} frontier molecular orbitals with the Fermi level of the metal, and the orientation of the molecule on the metal surface have been observed to determine high spread and low conductivities[10-12]. The examination of the amplitude and phase of frontier orbitals at the Fermi level within the cluster-molecule-cluster molecular complexes constitutes a significant analytical approach, which in recent developments[13] have demonstrated to be useful in examining the electron transport characteristics in molecular nanodevices[1-3,13]. For a weak bonding attraction between the C_{60} molecule and a metal electrode, the Fermi level of the silver-C_{60}-silver complexes has been identified within the HOMO and LUMO (frontier orbitals) energy range[14]. Furthermore, the most effective pathways for electron transport through π-delocalized systems are provided by the delocalized molecular orbitals that have appropriate symmetries and energy levels that closely aligned with the Fermi level[1-3].

For metal-molecule-metal systems, the research literature [1,15-21], indicates that the use of small models of metal clusters, to describe the nanocontact region between the metal cluster and the C_{60} molecule is of significant value, to understand the metal roughness effect in the fabrication and design of nanodevices. To investigate the bonding between the C_{60} molecule and silver surfaces, first principles calculations utilizing the $[Ag_{20}\text{-}C_{60}\text{-}Ag_{20}]^{n-}$ (where n = 0-3) molecular structures can be a highly effective approach. These studies could significantly enhance our understanding of the electron conduction mechanisms[5,9,10] involved when the C_{60} molecule bounces on a metal cluster surface[22].

The primary goal of this article is to analyze the bonding between the C_{60} molecule and two silver clusters utilizing the $[Ag_{20}\text{-}C_{60}\text{-}Ag_{20}]^{n-}$ (where n= 0-3) model systems. We will conduct density functional computations of the Ag-C_{60} complexes in several bonding modes, the HOMO-LUMO energy differences, the Fermi levels, and Mulliken charges.[4] The results of these findings will be compared with published results in similar Au-C_{60} complexes.[4] Additionally, we will analyze the amplitude and phase of molecular orbitals close to the Fermi level of the $[Ag_{20}\text{-}C_{60}\text{-}Ag_{20}]^{n}$ molecular structures. The insights gained from the analysis of the previously mentioned properties will lay the foundation for understanding the electron conduction characteristics of the silver-C_{60} interface.

Methology

To effectively describe the bonding interaction of the C_{60} molecule with a silver surface at either site, we utilized symmetric structures of the $[Ag_{20}\text{-}C_{60}\text{-}Ag_{20}]^{n-}$ (where n = 0-3) model complexes. These models mimic the bonding of the C_{60} molecule interacting with a pair of pyramidal-shaped silver clusters (Ag_{20}).

We studied four distinct bonding modes of the $[Ag_{20}\text{-}C_{60}\text{-}Ag_{20}]^{n-}$ (where n= 0-3) structures, as illustrated in Figure 1 which have the following spin multiplicities: for n= 0, the zero-charged singlet $[Ag_{20}\text{-}C_{60}\text{-}Ag_{20}]$ structure; for n= 1, the singly-charged doublet $[Ag_{20}\text{-}C_{60}\text{-}Ag_{20}]^{1-}$ structure; for n= 2, the doubly-charged singlet $[Ag_{20}\text{-}C_{60}\text{-}Ag_{20}]^{2-}$ structure and for n= 3, the triply-charged doublet $[Ag_{20}\text{-}C_{60}\text{-}Ag_{20}]^{3-}$ structure, correspondingly.

We utilized the density functional theory (DFT) with the Becke, 3-parameter, Lee-Yang-Parr (B3LYP) exchange-correlation functional[23,24], with Los Alamos National Laboratory effective core potential (ECP) and valence basis sets (LANL2DZ) [25, 26]. In our computations, while the carbon electrons were described using the Dunning/Huzinaga valence double-zeta (D95V) basis sets[27], Los Alamos (ECPs) were used to describe the electrons in the silver atoms. Gaussian 09 suite of codes[28] were used to conduct the calculations of all molecular geometries of this work. The energy minimization process began with the optimization of the bare C_{60} molecule, followed by the attachment and optimization of two silver clusters (Ag_{20}) to either side of the optimized C_{60} molecule. We minimize the energy of the $[Ag_{20}\text{-}C_{60}\text{-}Ag_{20}]^{n-}$ complexes through various bonding types, specifically: the η^1-$[Ag_{20}\text{-}C_{60}\text{-}Ag_{20}]^{n-}$, the $\eta^{1(b)}$-$[Ag_{20}\text{-}C_{60}\text{-}Ag_{20}]^{n-}$, the $\eta^1,\eta^{2(6)}$-$[Ag_{20}\text{-}C_{60}\text{-}Ag_{20}]^{n-}$ and the $\eta^{2(6)}$-$[Ag_{20}\text{-}C_{60}\text{-}Ag_{20}]^{n-}$ (where n= 0-3) structures. Where we have used the metal-C_{60} bond labeling conventions proposed by Lichtenberger and coworkers[29] to depict all the binding interaction types of molecular geometries in this work. All the structures were identified following the single labeling convention (η^1, $\eta^{2(6)}$, $\eta^{1(b)}$)[29] to identify two identical bonding sites at each side of the C_{60} molecule. When working with a structure that has two distinct bonding sites located at each side of the C_{60} molecule, a dual labeling convention is employed, denoted as (η^1, $\eta^{2(6)}$). The η^1-, $\eta^{2(6)}$-, $\eta^{1(b)}$- and η^1, $\eta^{2(6)}$- bonding structure types are described in Figure 1.

The molecular structures of all the $[Ag_{20}\text{-}C_{60}\text{-}Ag_{20}]^{n-}$ (where n= 0-3) structures will be compared with the optimized free C_{60} molecule to determine the changes in the structure of the C_{60} molecule [30] after the coordination of the silver clusters. To examine

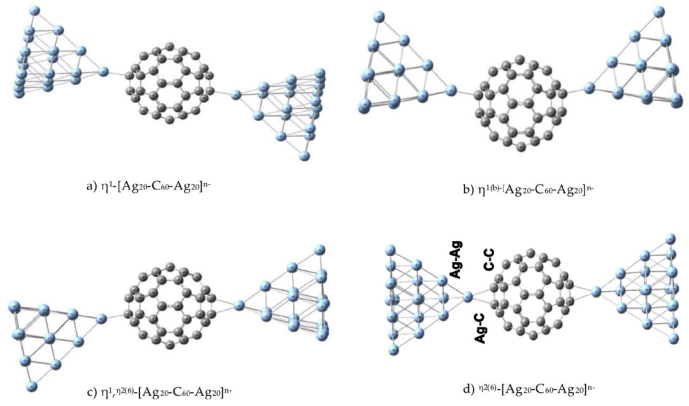

Figure 1. Different bonding modes of the $[Ag_{20}\text{-}C_{60}\text{-}Ag_{20}]^{n-}$(where n =0-3) complexes optimized at the DFT/B3LYP method with the LANL2DZ basis set: a) the σ-linearly bonded η^1-$[Ag_{20}\text{-}C_{60}\text{-}Ag_{20}]^{n-}$ complex, b) the σ-bent bonded $\eta^{1(b)}$-$[Ag_{20}\text{-}C_{60}\text{-}Ag_{20}]^{n-}$ complex, c) the σ-,π-bonded $\eta^1,\eta^{2(6)}$-$[Ag_{20}\text{-}C_{60}\text{-}Ag_{20}]^{n-}$ complex, and d) the π-linearly bonded $\eta^{2(6)}$-$[Ag_{20}\text{-}C_{60}\text{-}Ag_{20}]^{n-}$ complex. The C-C, the Ag-C, and the Ag-Ag describe the C_{60} C-C bond length of the two carbons in the fused six-member rings of C_{60} directly involved in the $Ag_{20}\text{-}C_{60}$ bonding site, the Ag-C_{60} bond length and the Ag_{20} Ag-Ag bond distance nearest to the $Ag_{20}\text{-}C_{60}$ bonding location, correspondingly.

the characteristics of the stationary points, the frequencies of all structures will be computed and evaluated. Furthermore, the Ag-C bond lengths, geometries, the HOMO-LUMO energy differences, the Fermi Levels, and the Mulliken charges will be also calculated and analyzed. The complexes Fermi level energies were all calculated following Morokuma's and coworkers' approximation[14,31,32], where the Fermi level energies can be approximated as the average energy of the HOMO and LUMO orbitals. This approximation is appropriate for molecular complexes with weak bonding between the C_{60} molecule and metal clusters[4]. To determine the aligning of the molecular orbital energies of the complexes with the Fermi level of the bare C_{60} molecule, we will examine the amplitude and phase of the orbitals near the frontier orbitals, as well as the Fermi levels of the complexes. This analysis will enable us to evaluate the electron transfer characteristics of the $[Ag_{20}\text{-}C_{60}\text{-}Ag_{20}]^{n-}$ (where n= 0-3) structures. This will be done by comparing these computed properties with the computed results for the $[Au_{20}\text{-}C_{60}\text{-}Au_{20}]^{n-}$ (where n= 0-3) complexes[4,5,30,33] and the free C_{60} molecule[34-36].

Results

The interaction between small silver clusters and the C_{60} molecule is believed to be weaker than the interaction between gold clusters and the C_{60} molecule[1]. The analysis of the Mulliken charges indicates that there is a transfer of charge from the Ag_{20} cluster to the C_{60} molecule. Electron conduction in the Ag-C_{60} complexes occurs through the π-charge cloud associated with the C-C bond, which overlaps with the Ag orbitals that have the right energy and symmetry. This also holds for electronic metal-C_{60} nanodevices[20]. Analysis of the frontier orbitals in the extended π-conjugated system has shown the significance of these orbitals in the charge transfer of molecular nanodevices[21]. The direction and amount of electron transport are associated with the properties of the HOMO and LUMO orbitals[1,13], especially in weak interaction complexes. The HOMO-LUMO energy differences of the $[Ag_{20}\text{-}C_{60}\text{-}Ag_{20}]^{n-}$ complexes are reduced compared to the estimated bulk bare C_{60} value of 1.95 eV, and the calculated value of 2.83 eV. The decrease in the HOMO-LUMO energy difference value of the complexes originates from the charge transfer from the Ag_{20} clusters to the C_{60} molecule.

To evaluate the molecular properties of the $[Ag_{20}\text{-}C_{60}\text{-}Ag_{20}]^{n-}$ (where n= 0-3) molecular structures, we carried out ab initio computations of molecular structures, Mulliken charges, the Fermi levels, and the HOMO-LUMO gaps. In Table 1, we show the computed properties utilizing the DFT/B3LYP/LANL2DZ level of theory. To facilitate energetic comparisons among the complexes, all the energies were referenced to the lower energy structure, the σ-bent bonded $\eta^{1(b)}$-$[Ag_{20}\text{-}C_{60}\text{-}Ag_{20}]^{2-}$ structure, for which the reference energy was set to 0.0 kcal/mol. This allows for a relative comparison of the energies to evaluate the effect of the charge of the complexes in the energies and to report the energies in a consistent framework. However by no means does this represent a formal comparison of the energies of all complexes with different numbers of electrons. The detailed analysis of the molecular structure parameters of the σ- and π-bonded $[Ag_{20}\text{-}C_{60}\text{-}Ag_{20}]^{n-}$ (where *n = 0-3*) structures suggest that at the $Ag_{20}\text{-}C_{60}$-bonding site, the Ag-Ag bond length in the Ag_{20} cluster, as well as the Ag-C bond lengths, are correlated inversely with the charge in the structures. Additionally, the C-C and C=C bond lengths for

all the structures were found to be longer than the corresponding experimentally reported distances of 1.464 and 1.405 Å[30] for the bare C_{60} molecule, correspondingly. This pattern agrees with the changes in the computed HOMO-LUMO energy differences, which decrease as the charge in the structures increases as indicated in Table 1. These very specific variations result from the changes in the electronic structures due to the changes in the electron distribution of the orbitals as the charge in the structures rises.

Zero-Charged [Ag_{20}-C_{60}-Ag_{20}] Singlet Complexes

We investigated the bonding between the Ag_{20} clusters and the zero-charged C_{60} molecule at the DFT/B3LYP/LANL2DZ method, focusing in four types of bonding: the η^1-[Ag_{20}-C_{60}-Ag_{20}], the $\eta^{1(b)}$-[Ag_{20}-C_{60}-Ag_{20}], the $\eta^1,\eta^{2(6)}$-[Ag_{20}-C_{60}-Ag_{20}] and the $\eta^{2(6)}$[Ag_{20}-C_{60}-Ag_{20}] for the singlet molecular structures. The first complex describes the σ-linear bonding shown in Figure 1(a), while the second represents the σ-bent bonding indicated in Figure 1(b). The third complex features the σ-, π-bonding, depicted in Figure 1(c), and the final complex is the π-linearly bonded structure illustrated in Figure 1(d). The relative energies of the η^1-[Ag_{20}-C_{60}-Ag_{20}], the $\eta^{1(b)}$-[Ag_{20}-C_{60}-Ag_{20}], the $\eta^1,\eta^{2(6)}$-[Ag_{20}-C_{60}-Ag_{20}] and the $\eta^{2(6)}$-[Ag_{20}-C_{60}-Ag_{20}] singlet structures are 109.2, 109.2, 110.3 and 111.6 kcal/mol above the lowest energy structure, correspondingly. The η^1-[Ag_{20}-C_{60}-Ag_{20}] singlet structure is characterized by a σ-linear bonding, where both Ag_{20} clusters are bonded in a pseudo-trans configuration to two carbon atoms situated in the fused six-member rings at either side of the C_{60} molecule, as shown in Figure 1(a). This bonding mode leads to two equal energy η^1-[Ag_{20}-C_{60}-Ag_{20}] conformations, interconnected by the $\eta^1,\eta^{2(6)}$-[Ag_{20}-C_{60}-Ag_{20}] complex, which serves as the transition state complex. In this structure, one of the Ag_{20} clusters is σ-linearly bonded to one carbon atom of C_{60} on one side, while the other Ag_{20} cluster is π-linearly bonded to the center of fused six-member rings of C_{60} on the other side, as illustrated in Figure 2. We have computed the Ag-C, the Ag-Ag, and the C-C bond lengths for the two carbons in the fused six-member rings of C_{60} directly associated with the Ag_{20}-C_{60} bonding site; these bond distances are illustrated in Figure 1(d).

Analysis of the C-C bond distance in the zero-charged complexes indicates that this bond distance changes between 1.411 and 1.418 Å. While the structure with the shortest bond length is the $\eta^{2(6)}$-[Ag_{20}-C_{60}-Ag_{20}] structure, the η^1-[Ag_{20}-C_{60}-Ag_{20}]

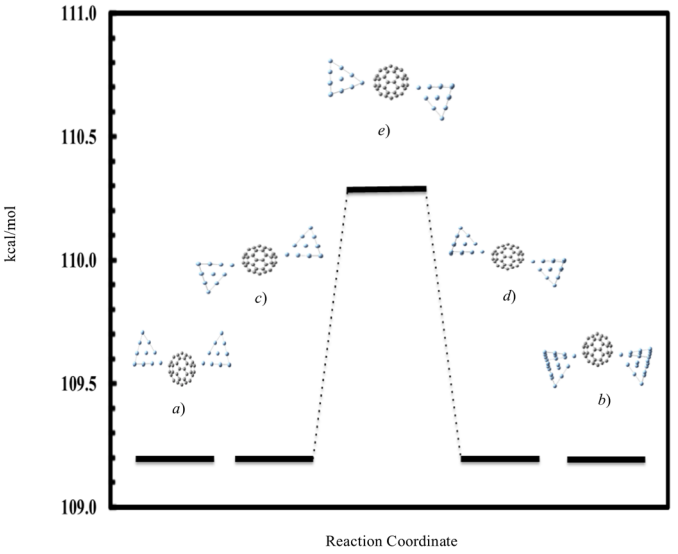

Figure 2 The interconversion reaction path of the zero-charged [Ag_{20}-C_{60}-Ag_{20}] singlet complexes computed at the DFT/B3LYP/LANL2DZ level of theory: a) and b) the degenerate σ-bent bonded $\eta^{1(b)}$-[Ag_{20}-C_{60}-Ag_{20}] structures, c) and d) the degenerate σ-linearly bonded η^1-[Ag_{20}-C_{60}-Ag_{20}] structures and e) the σ-,π-bonded $\eta^1,\eta^{2(6)}$-[Ag_{20}-C_{60}-Ag_{20}] transition state structure.

Table 1. Geometry and electronic structure parameters of the [Ag_{20}-C_{60}-Ag_{20}]$^{n-}$ (where *n* = 0-3) structures calculated at the DFT/B3LYP/LANL2DZ, and B3LYP/LANL2DZ//BHandHLYP/LANL2DZ methods.

Complex	Sym	[b]E_e kcal/ mol	[c]E_g eV	[d]E_F eV	[e]C-C Å	[e]Ag-C Å	[e]Ag-C Å	[e]Ag-Ag Å	Mulliken Charges[f]
$\eta^{1(b)}$-[Ag_{20}-C_{60}-Ag_{20}](s)	C_{2V}	109.2	1.98	-4.34	1.418	2.581	3.244	2.847	0.103
$\eta^{1(b)}$-[Ag_{20}-C_{60}-Ag_{20}]$^{1-}$(d)	C_{2V}	29.0	2.03	-2.06	1.437	2.462	3.091	2.857	-0.043
$\eta^{1(b)}$-[Ag_{20}-C_{60}-Ag_{20}]$^{2-}$(s)[a]	C_1	0.0	1.52	0.05	1.458	2.358	3.049	2.875	-0.260
$\eta^{1(b)}$-[Ag_{20}-C_{60}-Ag_{20}]$^{3-}$(d)	C_1	12.9	0.54	1.76	1.457	2.389	3.062	2.880	-0.718
η^1-[Ag_{20}-C_{60}-Ag_{20}](s)	C_{2h}	109.2	1.81	-4.42	1.418	2.585	3.246	2.847	0.102
η^1-[Ag_{20}-C_{60}-Ag_{20}]$^{1-}$ (d)	C_i	29.0	2.03	-2.06	3.082	2.463	3.082	2.857	-0.064
η^1-[Ag_{20}-C_{60}-Ag_{20}]$^{2-}$(s)	C_i	0.5	1.47	0.06	1.456	2.364	3.024	2.873	-0.257
η^1-[Ag_{20}-C_{60}-Ag_{20}]$^{3-}$(d)	C_i	13.2	0.29	1.48	1.456	2.397	3.048	2.878	-0.708
$\eta^{2(6)}$-[Ag_{20}-C_{60}-Ag_{20}] (s)	C_{2v}	111.6	1.83	-4.40	1.411	2.983	2.983	2.840	0.049
$\eta^{2(6)}$-[Ag_{20}-C_{60}-Ag_{20}]$^{1-}$(d)	C_{2V}	34.4	1.74	-2.02	1.411	2.983	2.983	2.840	-0.044
$\eta^{2(6)}$-[Ag_{20}-C_{60}-Ag_{20}]$^{2-}$(s)	C_{2v}	13.4	0.95	0.24	1.424	2.595	2.595	2.866	-0.248
$\eta^{2(6)}$-[Ag_{20}-C_{60}-Ag_{20}]$^{3-}$(d)	C_{2V}	15.6	0.52	1.67	1.457	2.550	2.550	2.864	-0.710
$\eta^1,\eta^{2(6)}$-[Ag_{20}-C_{60}-Ag_{20}](s)	C_1	110.3	1.80	-4.40	1.417	2.584	3.253	2.847	0.080
$\eta^1,\eta^{2(6)}$-[Ag_{20}-C_{60}-Ag_{20}]$^{1-}$(d)	C_1	30.0	2.03	-2.06	1.438	2.459	3.099	2.857	
$\eta^1,\eta^{2(6)}$-[Ag_{20}-C_{60}-Ag_{20}]$^{2-}$(s)	C_1	1.5	1.49	0.06	1.458	2.359	3.051	2.874	
$\eta^1,\eta^{2(6)}$-[Ag_{20}-C_{60}-Ag_{20}]$^{3-}$(d)	C_1	14.3	0.29	1.54	1.458	2.389	3.056	2.879	
Exp. C_{60} C-C[g] and E_g[h]	I_h		1.56[h],1.95[h]	-5.35	1.401[g](10), 1.458[g](6)				
Calc. Ag-C_{60}[i] and Ag-Ag[i]						2.570[i]		2.755[i]	

[a]Energies computed relative to the $\eta^{1(b)}$-[Ag_{20}-C_{60}-Ag_{20}]$^{2-}$(s) structure, letters in parenthesis indicate the multiplicity of the complexes. Sym stands for symmetry, [b]E^e the ground state energy, [c]E_g the computed HOMO-LUMO gaps and [d]E_F the calculated Fermi energy levels at the B3LYP/LANL2DZ//BHandHLYP/LANL2DZ method. [e]The C-C, Ag-C and Ag-Ag bond distances are referred to the Ag-C_{60} bonding site. [f]Mulliken charges are referred to each Ag_{20} cluster of symmetric structures. [g]The C-C experimental bond lengths of the bare C_{60} molecule with uncertainties in parentheses taken from Ref. 30, and [h]the HOMO-LUMO experimental gaps taken from Ref. 34-36. [i]The Ag-C bond calculated bond length value taken from Ref. 1, and the Ag-Ag bond length value from Ref. 37.

structure has the longest. This agrees with the energetic evidence that the π-bonded complex is a higher energy structure. The shorter C-C bond length is consequence of the weaker interaction with the silver clusters. From the comparison of the experimentally measured C-C bond length of 1.401 Å[30] for bare C_{60} molecules with the computed values of 1.411 Å and 1.418 Å for the zero-charged singlet structures, it is evident that the C-C bond distance is elongated in the complexes. The bond lengthening results due to the bonding with the silver clusters. The shortest C-C bond length in the $\eta^{2(6)}$-[Ag_{20}-C_{60}-Ag_{20}] structure indicates that the silver-C_{60} bonding for this structure is likely the weakest. The $\eta^{2(6)}$-[Ag_{20}-C_{60}-Ag_{20}] complex is symmetric, featuring two identical Ag-C bond lengths of 2.983 Å. In contrast, the η^{1}-[Ag_{20}-C_{60}-Ag_{20}] and the $\eta^{1(b)}$-[Ag_{20}-C_{60}-Ag_{20}] structures display two distinct Ag-C bond lengths: one short at 2.583 and one long at 3.245 Å. The bonding in the symmetric $\eta^{2(6)}$-[Ag_{20}-C_{60}-Ag_{20}] structure is distinctly different from the bonding in the η^{1}-[Ag_{20}-C_{60}-Ag_{20}] and the $\eta^{1(b)}$-[Ag_{20}-C_{60}-Ag_{20}] structures. The orbital analysis presented in Figure 6 indicates that in the $\eta^{2(6)}$-[Ag_{20}-C_{60}-Ag_{20}] structure the silver clusters bind through π-bonding with the C_{60} molecule.

The transition state structure labeled as $\eta^{1},\eta^{2(6)}$-[Ag_{20}-C_{60}-Ag_{20}] can be described as a mixture of the $\eta^{2(6)}$-[Ag_{20}-C_{60}-Ag_{20}] and η^{1}-[Ag_{20}-$C_{60}Ag_{20}$] structures. On one side the bonded silver atom displays one long Ag-C bond distance at 3.253 Å, and another short at 2.584 Å. On the other side, there are two identically short Ag-C bond distances at 2.972 Å. The Ag-Ag bond distance at the Ag_{20}-C_{60} bonding site shows small variation across the complexes, varying between 2.840 and 2.847 Å. In contrast, this distance is elongated when compared with the calculated Ag-Ag bond length of 2.755 Å for the bare Ag_{20} cluster[37]. These calculations agree with the Ag-Ag bond weakening when the Ag_{20} and the C_{60} form the Ag-C bond.

Singly-Charged [Ag_{20}-C_{60}-Ag_{20}]$^{1-}$ Doublet Complexes

Analogous computations, comparable to those of the zero-charged complexes, have been successfully conducted, utilizing the same theoretical method for the singly-charged [Ag_{20}-C_{60}-Ag_{20}]$^{1-}$ doublet molecular structures. The η^{1}-[Ag_{20}-C_{60}-Ag_{20}]$^{1-}$, the $\eta^{1(b)}$-[Ag_{20}-C_{60}-Ag_{20}]$^{1-}$, the $\eta^{1},\eta^{2(6)}$-[Ag_{20}-C_{60}-Ag_{20}]$^{1-}$ and the $\eta^{2(6)}$[Ag_{20}-C_{60}-Ag_{20}]$^{1-}$ doublet structures are found at 29.0, 29.0, 30.0 and 34.4 kcal/mol above the lowest energy structure, correspondingly. The η^{1}-[Ag_{20}-C_{60}-Ag_{20}]$^{1-}$ structure is characterized by a σ-linearly bonded structure, which leads to the existence of two equal energy η^{1}-[Ag_{20}-C_{60}-Ag_{20}]$^{1-}$ conformations. These two conformations are interconnected by the $\eta^{1},\eta^{2(6)}$-[Ag_{20}-C_{60}-Ag_{20}]$^{1-}$ structure, which serves as the transition state complex, as shown in Figure 3. The σ-linearly bonded η^{1}-[Ag_{20}-C_{60}-Ag_{20}]$^{1-}$ complex and the bonded σ-bent $\eta^{1(b)}$-[Ag_{20}-C_{60}-Ag_{20}]$^{1-}$ complex are nearly energy degenerate. Furthermore, the $\eta^{1},\eta^{2(6)}$-[Ag_{20}-C_{60}-Ag_{20}]$^{1-}$ complex has a lower energy than the symmetric π-linearly bonded $\eta^{2(6)}$-[Ag_{20}-C_{60}-Ag_{20}]$^{1-}$ complex. The latter represents a high energy maximum, suggesting that the [Ag_{20}-C_{60}-Ag_{20}]$^{1-}$ doublet structures exhibit a similar energy pattern to that of the zero-charged singlet structures.

We analyzed the bond distances between the Ag-C, the Ag-Ag, and the C_{60} C-C bonds of the two carbons located in the fused six-member rings of C_{60} and connected in the Ag_{20}-C_{60} bonding site, as depicted in Figure 1(d). For the [Ag_{20}-C_{60}-Ag_{20}]$^{1-}$doublet structures, the C-C bond lengths were calculated at approximately 1.411 Å and 1.438 Å. Comparison of these calculated values with the literature C_{60} C-C bond lengths of 1.401 Å[30] reveals the lengthening of the C-C bond distance in these structures. This is a direct consequence of the bonding of the C_{60} molecule with the silver clusters. The $\eta^{2(6)}$-[Ag_{20}-C_{60}-Ag_{20}]$^{1-}$ complex is the symmetric structure with two identical Ag-C bond lengths at 2.983 Å. In contrast, the η^{1}-[Ag_{20}-C_{60}-Ag_{20}]$^{1-}$ and the $\eta^{1(b)}$-[Ag_{20}-C_{60}-Ag_{20}]$^{1-}$ structures exhibit two distinct Ag-C bond lengths: one shorter bond at 2.463 Å and one longer bond at 3.00 Å. The bonding interaction in the $\eta^{2(6)}$-[Ag_{20}-C_{60}-Ag_{20}]$^{1-}$ structure are distinctly different from those in the η^{1}-[Ag_{20}-C_{60}-Ag_{20}]$^{1-}$ and the $\eta^{1(b)}$-[Ag_{20}-C_{60}-Ag_{20}]$^{1-}$ structures. As indicated by the orbitals shown in Figure 6, in the $\eta^{2(6)}$-[Ag_{20}-C_{60}-Ag_{20}]$^{1-}$ structure, the C_{60} molecule and the Ag_{20} clusters are π-bonded. The $\eta^{1},\eta^{2(6)}$-[Ag_{20}-C_{60}-Ag_{20}]$^{1-}$ transition state complex is a mixture of the $\eta^{2(6)}$-[Ag_{20}-C_{60}-Ag_{20}]$^{1-}$ and the η^{1}-[Ag_{20}-C_{60}-Ag_{20}]$^{1-}$ complexes, like zero-charged transition state of

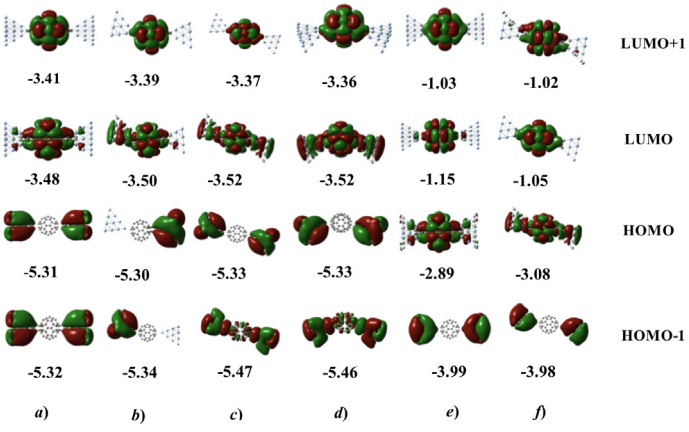

Figure 6. Calculated orbital energies of the orbitals near the frontier orbitals utilizing the DFT(B3LYP/LANL2DZ//BHandHLYP/LANL2DZ) level of theory for: a) the zero- charged $\eta^{2(6)}$-[Ag_{20}-C_{60}-Ag_{20}], b) the zero-charged $\eta^{1},\eta^{2(6)}$ -[Ag_{20}-C_{60}-Ag_{20}], c) the zero-charged η^{1}-[Ag_{20}-C_{60}-Ag_{20}], d) the zero-charged $\eta^{1(b)}$-[Ag_{20}-C_{60}-Ag_{20}], e) the singly-charged $\eta^{2(6)}$ -[Ag_{20}-C_{60}-Ag_{20}]$^{1-}$, and f) the singly-charged η^{1}-[Ag_{20}-C_{60}-Ag_{20}]$^{1-}$ structures, correspondingly. The energies of the orbitals are reported in eV, along with the corresponding plots with iso-value (0.002).

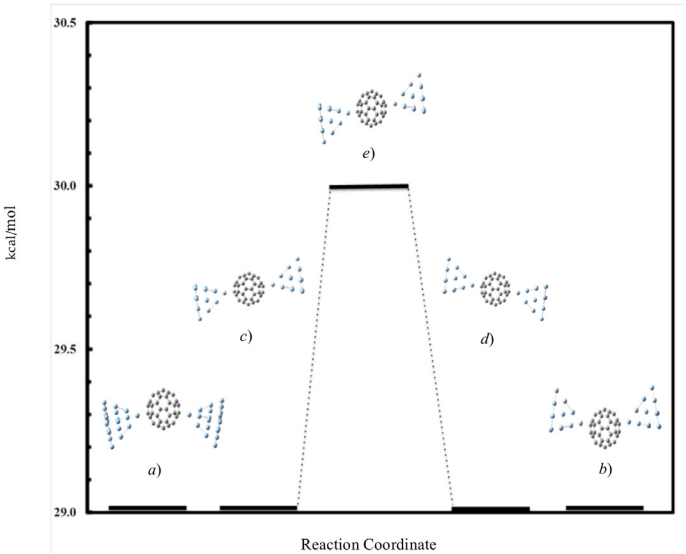

Figure 3. The interconversion reaction path of the singly-charged [Ag_{20}-C_{60}-Ag_{20}]$^{1-}$ doublet complexes computed at the DFT/B3LYP/LANL2DZ level of theory: a) and b) the degenerate σ-bent bonded $\eta^{1(b)}$-[Ag_{20}-C_{60}-Ag_{20}]$^{1-}$ structures, c) and d) the degenerate σ-linearly bonded η^{1}-[Ag_{20}-C_{60}-Ag_{20}]$^{1-}$ structures, and e) the σ-,π-bonded $\eta^{1},\eta^{2(6)}$-[Ag_{20}-C_{60}-Ag_{20}]$^{1-}$ transition state complex.

the previous section. As indicated in Figure 3, on one side displays two symmetrically positioned Ag-C bond lengths at 2.651 Å, while in the other side the bonded silver atom coordinates through two Ag-C bond distances of 2.459 Å and 3.099 Å, respectively. The calculations of the Ag-Ag bond distance at the Ag_{20}-C_{60} bonding site indicate small variations in the four structures from 2.840 to 2.857 Å, however, this distance is longer than the calculated Ag-Ag bond distance of 2.755 Å for the isolated Ag_{20} cluster[37], indicating that the Ag-Ag bond weakens when the Ag_{20} and the C_{60} form the Ag-C bond.

Doubly-Charged [Ag_{20}-C_{60}-Ag_{20}]$^{2-}$ Singlet Complexes

We have conducted similar calculations to those described earlier in the [Ag_{20}-C_{60}-Ag_{20}]$^{2-}$ singlet structures, utilizing the same bonding types and theoretical method. The relative energies of the η^1-[Ag_{20}-C_{60}-Ag_{20}]$^{2-}$, the $\eta^{1(b)}$-[Ag_{20}-C_{60}-Ag_{20}]$^{2-}$, the η^1,$\eta^{2(6)}$[Ag_{20}-C_{60}-Ag_{20}]$^{2-}$ and the $\eta^{2(6)}$-[Ag_{20}-C_{60}-Ag_{20}]$^{2-}$ singlet structures are 0.5, 0.0, 1.5 and 13.4 kcal/mol above the lowest energy structure, correspondingly. The η^1-[Ag_{20}-C_{60}-Ag_{20}]$^{2-}$ singlet structure is characterized by a σ-linear bonding of both Ag_{20} clusters to the C_{60} molecule in a pseudo-trans configuration, as was described in previous sections and depicted in Figure 1(a). This bonding type leads to two equal energy η^1-[Ag_{20}-C_{60}-Ag_{20}]$^{2-}$ conformations. These conformations are interconnected by the η^1,$\eta^{2(6)}$-[Ag_{20}-C_{60}-Ag_{20}]$^{2-}$ transition state structure with a barrier of 1kcal/mol. This structure is like the η^1,$\eta^{2(6)}$-zero-charged and singly-charged transition state structures of the previous sections and is shown in the interconversion path of Figure 4.

We have performed a detailed analysis of the Ag-C, the Ag-Ag, and the C_{60} C-C bond length of the two carbons in the fused six-member rings of C_{60} directly connected with the Ag_{20}-C_{60} bonding site, all these distances are illustrated in Figure 1(d). The C_{60} C-C bond length changes between 1.424 and 1.458 Å across the four doubly-charged singlet structures. While the $\eta^{2(6)}$-[Ag_{20}-C_{60}-Ag_{20}]$^{2-}$ complex exhibits the shortest bond distance, the $\eta^{1(b)}$-[Ag_{20}-C_{60}-Ag_{20}]$^{2-}$ complex has the longest bond length. This observation agrees with the σ-bent bonded complex being the lower energy structure, and the one with the stronger interaction between the Ag_{20} clusters and the C_{60} molecule, which results in a longer C-C distance. In contrast, our computed C_{60} C-C bond length values of 1.424 and 1.458 Å for the [Ag_{20}-C_{60}-Ag_{20}]$^{2-}$ singlet structures are longer than the measured C_{60} C-C distance value of 1.401 Å (30). This makes evident that the C-C bond distance lengthening is a consequence of the Ag-C_{60} bonding interaction. Similarly to the previous sections, the $\eta^{2(6)}$-[Ag_{20}-C_{60}-Ag_{20}]$^{2-}$ structure is a symmetric structure, featuring two identical Ag-C bond lengths of 2.595 Å. In contrast, the η^1-[Ag_{20}-C_{60}-Ag_{20}]$^{2-}$ and the $\eta^{1(b)}$-[Ag_{20}-C_{60}-Ag_{20}]$^{2-}$ structures exhibit two different Ag-C bond lengths, one shorter at 2.361, and one longer at 3.065 Å. The analysis of the molecular orbitals in the $\eta^{2(6)}$-[Ag_{20}-C_{60}-Ag_{20}]$^{2-}$ structure shows that the Ag_{20} clusters and the C_{60} molecule bind through π-bonding. This result indicates that the bonding interaction differs significantly in the symmetric $\eta^{2(6)}$-[Ag_{20}-C_{60}-Ag_{20}]$^{2-}$ structure compared with the η^1-[Ag_{20}-C_{60}-Ag_{20}]$^{2-}$ and $\eta^{1(b)}$-[Ag_{20}-C_{60}-Ag_{20}]$^{2-}$ structures. The η^1,$\eta^{2(6)}$-[Ag_{20}-C_{60}-Ag_{20}]$^{2-}$ structure conforms to the same pattern of the [Ag_{20}-C_{60}-Ag_{20}]$^{1-}$ complexes described previously. This is the transition state structure and can be described as a mixture of the $\eta^{2(6)}$-[Ag_{20}-C_{60}-Ag_{20}]$^{2-}$ and η^1-[Ag_{20}-C_{60}-Ag_{20}]$^{2-}$ structures. While in one side displays a longer Ag-C bond distance at 3.051 Å, and another shorter bond distance at 2.359 Å, on the other side shows two identically shorter Ag-C bond lengths at 2.524 Å. The Ag-Ag bond length at the Ag_{20}-C_{60} bonding site exhibits small changes across the four structures, with values changing from 2.866 to 2.875 Å. However, this bond is elongated with respect to the calculated Ag-Ag distance at 2.755 Å for the free Ag_{20} cluster[37]. This observation reflects the debilitation of the Ag-Ag bond caused by the formation of the Ag-C_{60} bond.

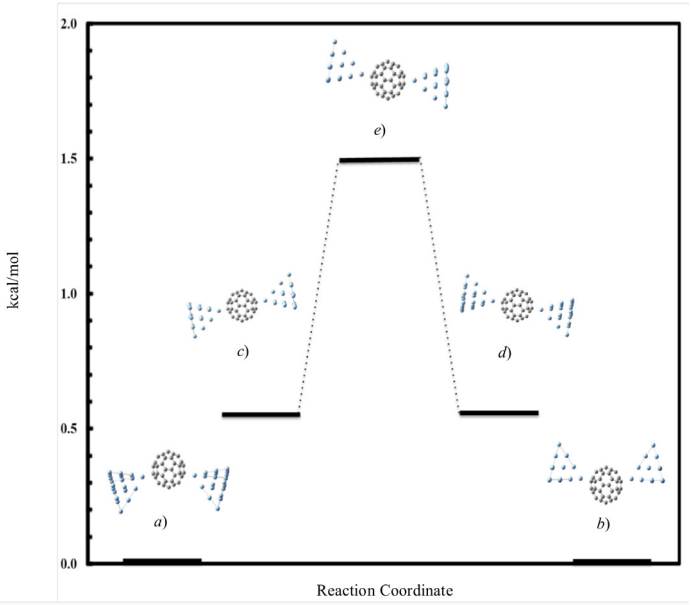

Figure 4. The interconversion reaction path of the doubly-charged [Ag_{20}-C_{60}-Ag_{20}]$^{2-}$ singlet complexes computed at the DFT/B3LYP/LANL2DZ level of theory: a) and b) the degenerate σ-bent bonded $\eta^{1(b)}$-[Ag_{20}-C_{60}-Ag_{20}]$^{2-}$ structures (the lowest energy structure), c) and d) the degenerate σ-linearly bonded η^1-[Ag_{20}-C_{60}-Ag_{20}]$^{2-}$ structures, and e) the σ-,π-bonded η^1,$\eta^{2(6)}$-[Ag_{20}-C_{60}-Ag_{20}]$^{2-}$ transition state complex.

Although the singlet $\eta^{1(b)}$-[Ag_{20}-C_{60}-Ag_{20}]$^{2-}$ and the doublet $\eta^{1(b)}$-[Ag_{20}-C_{60}-Ag_{20}]$^{3-}$ structures are closer in energy compared with the other doubly charged molecular structures, the $\eta^{1(b)}$-[Ag_{20}-C_{60}-Ag_{20}]$^{2-}$ structure was identified as the lowest energy structure (global minimum). In this structure, the two Ag_{20} clusters are bonded to the C_{60} molecule creating two pseudo-cis configurations, as was described in analogous complexes of the previous sections, this structure is indicated in Figure 1(b).The $\eta^{1(b)}$-[Ag_{20}-C_{60}-Ag_{20}]$^{2-}$ singlet structure is approximately 12 kcal/mol lower in energy than the $\eta^{1(b)}$-[Ag_{20}-C_{60}-Ag_{20}]$^{3-}$ doublet structure and 30 kcal/mol more stable than the doublet $\eta^{1(b)}$-[Ag_{20}-C_{60}-Ag_{20}]$^{1-}$ structure discussed previously. This increment in the stability of the $\eta^{1(b)}$-[Ag_{20}-C_{60}-Ag_{20}]$^{2-}$ singlet complex compared to the $\eta^{1(b)}$-[Ag_{20}-C_{60}-Ag_{20}]$^{1-}$ doublet complex can be attributed, in part, to the pairing of all electrons within the $\eta^{1(b)}$-[Ag_{20}-C_{60}-Ag_{20}]$^{2-}$ singlet structure. Additionally, there is a stronger electrostatic interaction between the C_{60} molecule and the Ag_{20} clusters in the $\eta^{1(b)}$-[Ag_{20}-C_{60}-Ag_{20}]$^{2-}$ singlet complex, as emphasized by the computed Mulliken charges, indicated in Table 1. Moreover, when comparing the $\eta^{1(b)}$-[Ag_{20}-C_{60}-Ag_{20}]$^{2-}$ singlet structure with the $\eta^{1(b)}$-[Ag_{20}-C_{60}-Ag_{20}]$^{3-}$ doublet structures, it becomes evident that the doubly-charged singlet structures are more stable. This stability is influenced by the Coulombic attraction between the C_{60} molecule and the silver clusters, and the multiplicity of spin of the $\eta^{1(b)}$-[Ag_{20}-C_{60}-Ag_{20}]$^{n-}$ complexes (where n = 2,3). Although the electrostatic attraction between the Ag_{20} clusters and the C_{60} molecule is stronger in the triply-charged doublet structures, and the unpaired electron in

these structures appears to be more delocalized compared with the doubly-charged singlet structures, the unpaired electron goes into a higher energy orbital. This makes the $\eta^{1(b)}$-[Ag_{20}-C_{60}-Ag_{20}]$^{3-}$ doublet complex a higher energy structure than the $\eta^{1(b)}$-[Ag_{20}-C_{60}-Ag_{20}]$^{2-}$ singlet complex, with all its electrons paired up in localized lower energy orbitals.

Triply-Charged [Ag_{20}-C_{60}-Ag_{20}]$^{3-}$ Doublet Complexes

The computations in the [Ag_{20}-C_{60}-Ag_{20}]$^{3-}$ doublet complexes at the DFT/B3LYP/LANL2DZ level indisputably validate the occurrence of four distinct kinds of structures analogous to those previously discussed. Although the [Ag_{20}-C_{60}-Ag_{20}]$^{3-}$ structures coexist as doublet or quartet structures, we will be discussing only the doublet complexes in this work. The η^1-[Ag_{20}-C_{60}-Ag20]$^{3-}$, the $\eta^{1(b)}$-[Ag_{20}-C_{60}-Ag_{20}]$^{3-}$, the η^1,$\eta^{2(6)}$-[Ag_{20}-C_{60}-Ag_{20}]$^{3-}$ and the $\eta^{2(6)}$-[Ag_{20}-C_{60}-Ag_{20}]$^{3-}$ doublet structures are situated 13.2, 12.9, 14.3 and 15.6 kcal/mol higher than the lower energy structure, correspondingly. The doublet σ-bent bonded $\eta^{1(b)}$-[Ag_{20}-C_{60}-Ag_{20}]$^{3-}$ structure is 12.9 kcal/mol above the lower energy structure. In this structure, the C_{60} molecule is bonded on each side by the two Ag_{20} clusters in a pseudo-cis configuration, as was described in previous sections and depicted in Figure 1(b). In contrast, the η^1-[Ag_{20}-C_{60}-Ag_{20}]$^{3-}$ structure is a σ-linearly bonded structure located 13.2 kcal/mol above the lower energy structure. In this structure, both Ag_{20} clusters are bonded in a pseudo-trans configuration to one carbon atom at either side of the C_{60} molecule, as illustrated in Figure 1(a). This bonding interaction results in two equal energy η^1-[Ag_{20}-C_{60}-Ag_{20}]$^{3-}$ conformations, interconnected by the η^1,$\eta^{2(6)}$-[Ag_{20}-C_{60}-Ag_{20}]$^{3-}$ complex located 14.3 kcal/mol above the lowest energy complex. This structure represents the transition state structure, and it is illustrated in Figure 5. The $\eta^{2(6)}$-[Ag_{20}-C_{60}-Ag_{20}]$^{3-}$ complex is a higher-order maximum located 13.4 kcal/mol higher than the lowest energy complex. The former structure has two imaginary frequencies: one interconnects the two pseudo-trans degenerate η^1-[Ag_{20}-C_{60}-Ag_{20}]$^{3-}$ conformations and the other interconnects the two pseudo-cis equal energy $\eta^{1(b)}$-[Ag_{20}-C_{60}-Ag_{20}]$^{3-}$ conformations.

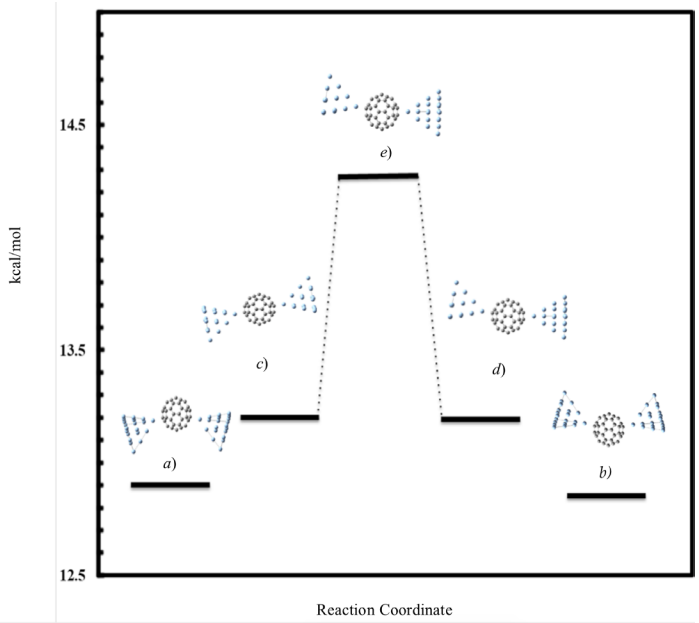

Figure 5. The interconversion reaction path of the triply-charged [Ag_{20}-C_{60}-Ag_{20}]$^{3-}$ doublet complexes computed at the DFT/B3LYP/LANL2DZ level of theory: a) and b) the degenerate σ-bent bonded $\eta^{1(b)}$-[Ag_{20}-C_{60}-Ag_{20}]$^{3-}$ structures, c) and d) the degenerate σ-linearly bonded η^1-[Ag_{20}-C_{60}-Ag_{20}]$^{3-}$ structures, and e) the σ-,π-bonded η^1,$\eta^{2(6)}$-[Ag_{20}-C_{60}-Ag_{20}]$^{3-}$ transition state complex.

To gain insight into the nature of the Ag-C_{60} bonding, we calculated the bond lengths of Ag-C, Ag-Ag, and the C_{60} C-C bond length of two carbons located in the fused six-member rings of the C_{60} molecule along the Ag_{20}-C_{60} bonding site, as illustrated in Figure 1(d). The C_{60} C-C bond distance within the triply-charged structures vary in the range of 1.456 and 1.458 Å. The η^1-[Ag_{20}-C_{60}-Ag_{20}]$^{3-}$ structure exhibits the longest bond distance, while the $\eta^{2(6)}$-[Ag_{20}-C_{60}-Ag_{20}]$^{3-}$ structure has the shortest. A weaker bonding between the silver clusters and the C_{60} molecule in the $\eta^{2(6)}$-[Ag_{20}-C_{60}-Ag_{20}]$^{3-}$ structure leads to a longer C_{60} C-C bond length, this observation reinforces the notion that the π-bonded structure is a higher energy structure. Experimentally, the C_{60} C-C bond length is reported to be 1.401 Å (30) for the bare C_{60} molecule, whereas the calculated values for the [Ag_{20}-C_{60}-Ag_{20}]$^{3-}$ structures fall within the range of 1.456 to 1.458 Å. This difference indicates an elongation of the C-C bond distance in the structures due to the bonding between the C_{60} and the silver clusters. The $\eta^{2(6)}$-[Ag_{20}-C_{60}-Ag_{20}]$^{3-}$ complex is symmetric structure, featuring two equal Ag-C bond lengths of 2.550 Å. The molecular orbitals suggest that in the $\eta^{2(6)}$-[Ag_{20}-C_{60}-Ag_{20}]$^{3-}$ complex, the C_{60} molecule interacts with the Ag_{20} clusters through π-bonding. Furthermore, the shorter C_{60} C-C bond distance directly involved in the Ag-C bond further reinforces the idea that the silver-C_{60} interaction for this structure is likely the weakest. On the other hand, the η^1-[Ag_{20}-C_{60}-Ag_{20}]$^{3-}$ and the $\eta^{1(b)}$-[Ag_{20}-C_{60}-Ag_{20}]$^{3-}$ structures both exhibit two distinct Ag-C bond lengths: one shorter approximately along 2.393 Å, and one longer at 3.055 Å. This pattern suggests that the bonding interaction in the symmetric $\eta^{2(6)}$-[Ag_{20}-C_{60}-Ag_{20}]$^{3-}$ structure is very different from those present in the η^1-[Ag_{20}-C_{60}-Ag_{20}]$^{3-}$ and $\eta^{1(b)}$-[Ag_{20}-C_{60}-Ag_{20}]$^{3-}$ complexes.

The η^1,$\eta^{2(6)}$-[Ag_{20}-C_{60}-Ag_{20}]$^{3-}$ transition state complex can be a described as a mixture of the $\eta^{2(6)}$-[Ag_{20}-C_{60}-Ag_{20}]$^{3-}$ and η^1-[Ag_{20}-C_{60}-Ag_{20}]$^{3-}$ structures. One side of this structure exhibits a short Ag-C bond distance at 2.389 Å and another long at 3.056 Å, while on the other side two equal Ag-C bond distances at 2.567 Å. The Ag-Ag bond distance at the Ag_{20}-C_{60} bonding location varies narrowly among the four structures, changing from 2.866 to 2.880 Å. However, this bond is elongated compared with the calculated Ag-Ag bond length of 2.755 Å for the bare Ag_{20} cluster[37], which suggests that the Ag-Ag bond weakens when the Ag_{20} and C_{60} form the Ag-C bond.

The Analysis of the Frontier Orbitals for the [Ag_{20}-C_{60}-Ag_{20}]$^{n-}$ (where n= 0,1) complexes

Several research works have utilized the analysis of the frontier orbitals to study electron transfer in metal-C_{60}-metal systems[13,38]. It is well established that metal-organic molecule junctions with weak coupling demonstrate effective electron conduction routes via π-localized and delocalized molecular orbitals close to the Fermi level[1,13, 38]. In these molecular complexes, the probabilities for direction and transmission of electron transport are significantly shaped by the phase and amplitude of the frontier orbitals situated near the Fermi level[1,13].

In molecular complexes where metal clusters interact weakly with the C_{60} molecule, we can assume that the frontier orbitals of the complexes, which are close to the C_{60} Fermi level, will be like those of the bare C_{60} molecule[13]. In contrast, if the Ag_{20} clusters

interact strongly with the C_{60} molecule through stronger bonds, the frontier molecular orbitals of the resulting molecular complex will be substantially different in both shape and energy from those of the bare C_{60} molecule. Our ongoing research has generated results corroborating this assumption based on molecular complexes previously studied[4]. Like the gold-C_{60} complexes[4], the relative energies and the Ag-C interacting bond lengths of the $[Ag_{20}\text{-}C_{60}\text{-}Ag_{20}]^n$ (where *n*= 0-3) complexes clearly indicate in Table 1 that the weakest complexes are the zero-charged and singly-charged structures. Additionally, from all the studied σ- and π-bonded molecular complexes, the symmetrical π-linearly bonded $\eta^{2(6)}[Ag_{20}\text{-}C_{60}\text{-}Ag_{20}]^{n-}$ (where *n*= 0-3) structures are the weakest complexes. As a result of this, these complexes are the most interesting for studying and analyzing the electron transfer characteristics of the frontier orbitals of the $[Ag_{20}\text{-}C_{60}\text{-}Ag_{20}]^{n-}$ (where *n*= 0-3) molecular structures. These molecular complexes are particularly exciting because they are the weakest bonded structures with π-delocalized molecular orbitals, which makes the analysis of the frontier orbitals easier and more direct.

The electron populations, the Mulliken charges, and the orbitals energies were calculated at the BHandHLYP/LANL2DZ method utilizing the molecular structures optimized at the B3LYP/LANL2DZ method. This combined method[23,39], hereafter will be alluded to as the B3LYP/LANL2DZ//BHandHLYP/LANL2DZ level of theory. The computed HOMO, HOMO-1, LUMO, and LUMO+1 molecular orbitals for the η^1-$[Ag_{20}\text{-}C_{60}\text{-}Ag_{20}]$, the $\eta^{1(b)}$-$[Ag_{20}\text{-}C_{60}\text{-}Ag_{20}]$, the $\eta^1,\eta^{2(6)}$-$[Ag_{20}\text{-}C_{60}\text{-}Ag_{20}]$, and the $\eta^{2(6)}$-$[Ag_{20}\text{-}C_{60}\text{-}Ag_{20}]$ zero-charged singlet structures; and for the $\eta^{2(6)}$-$[Ag_{20}\text{-}C_{60}\text{-}Ag_{20}]^1$, and the η^1-$[Ag_{20}\text{-}C_{60}\text{-}Ag_{20}]^{1-}$ singly-charged doublet structures are depicted in Figure 6. A detailed analysis of the orbitals' energies near the frontier orbitals suggests that the HOMO, HOMO-1, LUMO, and LUMO+1 orbitals for the zero-charged singlet structures are in the energy limits of -5.33 to -3.41 eV. In the zero- charged structures, only the LUMO and HOMO-1 orbitals are fully delocalized throughout the complexes. The LUMO orbital for the $\eta^1,\eta^{2(6)}$-$[Ag_{20}\text{-}C_{60}\text{-}Ag_{20}]$ transition state structure with the energy of -3.50 eV, is partially delocalized along the symmetric π-bonded side of the structure. This suggests that for the zero-charged structures, at the B3LYP/LANL2DZ// BHandHLYP/LANL2DZ method, only the HOMO, HOMO-1, and the LUMO orbitals fall near the energy limit of -5.35 eV, the Fermi level of the C_{60} molecule. Although the analysis of the orbital energies and delocalization patterns for the singly-charged structures indicate that the HOMO-1, HOMO, LUMO, and LUMO+1 orbitals are also delocalized through the η^1-$[Ag_{20}\text{-}C_{60}\text{-}Ag_{20}]^{1-}$ and the $\eta^{2(6)}$-$[Ag_{20}\text{-}C_{60}\text{-}Ag_{20}]^{1-}$ molecular complexes, the orbital energies are in the limits of -3.99 eV to -1.02 eV, which is significantly far from the Fermi level of the zero-charged free C_{60} molecule.

Compared to the zero-charged structures, in the single-charged complexes, the orbital energies of the HOMO, HOMO-1, LUMO, and LUMO+1 orbitals are far away from the Fermi level of the free C_{60} molecule. This is the result of the Coulombic attraction between the C_{60} molecule and the Ag_{20} clusters in the $[Ag_{20}\text{-}C_{60}\text{-}A_{20}]^{1-}$ complexes which increases as the charge in the complexes rises. This effect differs quite significantly in the zero-charged complexes, for which the weaker interaction between the C_{60} and the silver clusters results in the frontier orbitals weakly influenced by the bonding interaction. This in consequence results with energies in the range of the Fermi level of the bare C_{60} molecule. This detailed analysis suggests that at the B3LYP/LANL2DZ//BHandHLYP/LANL2DZ method, the $[Ag_{20}\text{-}C_{60}\text{-}Ag_{20}]$ singlet complexes have the best orbitals for electron transport through the $Ag_{20}\text{-}C_{60}\text{-}Ag_{20}$ system, as illustrated in Figure 6. The $[Ag_{20}\text{-}C_{60}\text{-}Ag_{20}]$ structures exhibit delocalized molecular orbitals that extend through the entire complex and correspond to the energy levels near the Fermi level of the bare C_{60} molecule. This offers a valuable opportunity to enhance our understanding of electron transport at the $Ag_{20}\text{-}C_{60}\text{-}Ag_{20}$ interface.

Conclusion

To assess all the bonding types and molecular properties of the $Ag_{20}\text{-}C_{60}\text{-}Ag_{20}$ bonding interaction, we have conducted first principles molecular orbital computations in the $[Ag_{20}\text{-}C_{60}\text{-}Ag_{20}]^{n-}$ (where *n*= 0-3) complexes using the DFT/B3LYP/LanL2DZ method. Our computations show that the σ-bent bonded $\eta^{1(b)}$-$[Ag_{20}\text{-}C_{60}\text{-}Ag_{20}]^{2-}$ singlet complex is the lowest energy structure. This is followed in stability by the $\eta^{1(b)}$-$[Ag_{20}\text{-}C_{60}\text{-}Ag_{20}]^{3-}$ doublet, the $\eta^{1(b)}$-$[Ag_{20}\text{-}C_{60}\text{-}A_{20}]^{1-}$ doublet, and lastly by the $\eta^{1(b)}$-$[Ag_{20}\text{-}C_{60}\text{-}Ag_{20}]$ singlet structure. Similar behavior is followed by the linearly σ-bonded η^1-$[Ag_{20}\text{-}C_{60}\text{-}Ag_{20}]^{n-}$ (where *n*= 0-3) structures. The above stability is the result of the growing electrostatic interaction between the C_{60} molecule, and the Ag_{20} clusters as the charge in the η^1-$[Ag_{20}\text{-}C_{60}\text{-}Ag_{20}]^{n-}$ (where *n*= 0-3) structures increases. Similar stability order is followed by the gold-C_{60} complexes[4].

We computed the molecular orbitals close to the frontier orbitals for the $[Ag_{20}\text{-}C_{60}\text{-}Ag_{20}]^{n-}$ (where *n* = 0, 1) complexes using the DFT/B3LYP and BHandHLYP methods, and the LANL2DZ basis sets. The results clearly showed that the $\eta^{2(6)}$-$[Ag_{20}\text{-}C_{60}\text{-}Ag_{20}]$, the $\eta^1,\eta^{2(6)}$-$[Ag_{20}\text{-}C_{60}\text{-}Ag_{20}]$, the η^1-$[Ag_{20}\text{-}C_{60}\text{-}Ag_{20}]$, and the $\eta^{1(b)}$-$[Ag_{20}\text{-}C_{60}\text{-}Ag_{20}]$ structures have delocalized orbitals close to the HOMO and LUMO orbitals with Fermi levels energies of -4.40, -4.43, -4.43, -4.43 eV, correspondingly. These energy levels are all less than 1eV above the Fermi level of -5.35 eV for the bare C_{60} molecule, which was also calculated using the same theoretical approach. The HOMO orbitals in these complexes are energy degenerate with a large contribution from the C_{60} molecule h_u symmetry HOMO, which gives these complexes a unique versatile ground electron configuration. Also, the HOMO-LUMO gaps in these complexes were found to be lower than those of the corresponding zero-charge gold-C_{60} complexes. This implies a lower barrier for electron transfer and needs to be investigated further using large silver clusters to establish this fact.

Acknowledgments

We thank the support of the NSF under grant number OCI-1053575, XSEDE and the ITS at Fayetteville State University.

References

1. Shukla, M.K.; Dubey, M.; Zakar, E.; Leszczynski, J. *J. Phys. Chem. C.* **2012**, *116*, 1966-1972.
2. Shukla, M.K.; Dubey, M.; Zakar, E.; Leszczynski, J. *J. Phys. Chem. C.* **2009**, *113*, 11351-11357.
3. Shukla, M.K.; Dubey, M.; Leszczynski, J. *J. ACS Nano* **2008**, *2*, 227-234.
4. Castillo-Chará, J. *Comput. Theor. Chem.* **2020**, *1187*, 112918.
5. Park, H.P.; Park, J.; Lim, A.K.L.; Anderson, E.; Alivisatos,

A.P.; McEuen, P.L. *Nature* **2000**, *407*, 57-60.
6. Chen, L.; Chen, W.; Huang, H.; Zhang, H.L.; Yuhara, J.; Wee, A.T.S. *Adv. Mater* **2008**, *20*, 484.
7. Ward, D.R.; Halas, N.J.; Ciszek, J.W.; Tour, J.M.; Wu, Y.; Nordlander, P.; Natelson, D. *Nano Lett.* **2008**, *8* (3), 919-924.
8. Jamelah, Al-O. S.; Sheena, M. Y.; Shyma, M. Y.; Nivedita, A.; Abdulaziz A., Al-S.; Gamberini, M. C. *J. Comput. Biophys. Chem.* **2024**, *23*(01), 47-61.
9. Yee, S.K.; Malen, J.A; Majumdar, A.; Segalman, R. *Nano Lett.* **2011**, *11*, 4089-4094.
10. Lu, X.H.; Grobis, M.; Khoo, K.H.; Louie, S.G.; Crommie, M.F. *Phys. Rev. Lett.* **2003**, *90*, 096802.
11. Lu, X.H.; Grobis, M.; Khoo, K.H.; Louie, S.G.; Crommie, M.F. *Phys. Rev. B*. **2004**, *70*, 115418-4-115418-8.
12. Neel, N.; Kroger, Jr.; Limot, L.; Berndt, R. *Nano Lett. **2008***, *8* (5), 1291–1295.
13. Yoshizawa, K.; Tada, T.; Staykov, A. *J. Am. Chem. Soc.* **2008**, *130*, 9406-9413.
14. Witek, H.A; Irle, S.; Zheng, G.; De Jong, W.A.; Morokuma, K. *J. Chem. Phys*. **2006**, *125*, 214706.
15. Muniz-Miranda, M.; Cardini, G.; Schettino, V. *Theor. Chem. Acc.* **2004**, *111*(2), 264-269.
16. Cardini, G.; Muniz-Miranda, M. *J. Phys. Chem. B.* **2002**, *106*, 6875-6880.
17. Yuan, L-F.; Yang; Li, J.Q.; Zhu, Q-S. *Phys. Rev. B.* **2001**, *65*, 035415.
18. Chase, S.J.; Bacsa, W.S; Mitch, M. G.; Pilione, L.J.; Lannin, J.S. *Phys. Rev. B.* **1992**, *46*, 7873-7877.
19. Ohno, T.R.; Chen, Y.; Harvey, S.E.; Kroll, G.H; Weaver, J.H. *Phys. Rev. B.* **1991**, *44*, 13747-13755.
20. Bagus, P.S; Woll, C. *Chem. Phys. Lett.* **1998**, *294*, 599-604.
21. van Daelen, M.A.; Li, Y.S.; Newsan, J.M.; Van Santen, R.A. *J. Phys. Chem*. **1994**, *100*, 2279-2289.
22. Dresselhaus, M.S; Dresselhaus, G.; Eklund, P.C. *Science of Fullerenes and Carbon Nanotubes*; first ed., Academic: New York, US, **1996**, pp. 556-648.
23. Lee, C.; Yang, W.; Parr, R.G. *Phys. Rev. B.* **1988**, *37*, 785-789.
24. Becke, A.D. *J. Chem. Phys*. **1993**, *98*, 5648-5652.
25. Hay, P.J.; Wadt, W.R. *J. Chem. Phys.* **1985**, *82*, 270-283.
26. Wadt, W.R.; Hay, P.J. *J. Chem. Phys*. **1985**, *82*, 284-298.
27. Dunning, Jr. T. H.; Hay, P.J. *In Modern Theoretical Chemistry*, Ed. H. F. Schaefer III, Vol. 3, Plenum, New York, **1977**, pp. 1-28.
28. Frisch, M.J.; Trucks, G.W.; Schlegel, H.B.; Scuseria, G.E.; Robb, M.A.; Cheeseman, J.R.; Scalmani, G.; Barone, V.; Mennucci, B.; Petersson, G.A.; Nakatsuji, H.; Caricato, M.; Li, X.; Hratchian, H. P.; Izmaylov A.F.; Bloino, J.; Zheng, G.; Sonnenberg, J.L.; Hada, M.; Ehara, M.; Toyota, K.; Fukuda, R.; Hasegawa, J.; Ishida, M.; Nakajima, T.; Honda, Y.; Kitao, O.; Nakai, H.; Vreven, T.; Montgomery, J.; J.E. Peralta, J.A.; Ogliaro, F.; Bearpark, M.; Heyd, J.J.; Brothers, E.; Kudin, K.N.; Staroverov, V.N.; Kobayashi, R.; Normand, J.; Raghavachari, K.; Rendell, A.; Burant, J.C.; Iyengar, S.S.; Tomasi, J.; Cossi, M.; Rega, N.; Millam, J.M.; Klene, M.; Knox, J.E.; Cross, J.B.; Bakken, V.; Adamo, C.; Jaramillo, J.; Gomperts, R.; Stratmann, R.E.; Yazyev, O.; Austin, A.J.; Cammi, R.; Pomelli, C.; Ochterski, J.W.; Martin, R.L.; Morokuma, K.; Zakrzewski, V.G.; Voth, G.A.; Salvador, P.; Dannenberg, J.J.; Dapprich, S.; Daniels, A.D.; Farkas, Ö.; Foresman, J.B.; Ortiz, J.V.; Cioslowski, J.;. Fox. D.J. *Gaussian 09, Revision E.01. Gaussian Inc: Wallingford, CT*, **2013**.
29. Lichtenberger, D.L.; Wright, L.L.; Gruhn, N.E.; Rempe, M.E. *Synthetic Metals* **1993**, *59*, 353-367.
30. Hedberg, K.; Hedberg, L.; Bethune, D.S.; Brown, C.A.; Dorn, H.C.; Johnson, R.D.; De Vries, M. *Science* **1991**, *254*, 410412.
31. Al-Aaraji, N.AH.; Hashim, A.; Abduljalil, H.M.; Hadi, A. *Opt. Quant. Electron*. **2023**, *55*, 743. https://doi.org/10.1007/s11082-023-05048-5
32. Yu, J.; Su, N. Q.; Yang, W. *JACS Au*. **2022**, *2*(6), 1383–1394. 10.1021/jacsau.2c00085.
33. Liang, W.; Bockrath, M.; Bozovic, D.; Hafner, J.H.; Tinkham, M.; Park, H. *Nature* **2001**, *411*, 665.
34. Hare, J.P; Kroto, H.W.; Taylor, R. *Chem. Phys. Lett.* **1991**, *177*, 394-398.
35. Skumanich, A. *Chem. Phys. Lett.* **1991**, *182*, 486-490.
36. Hung, R.R.; Grabowski, J.J. *J. Phys. Chem.* **1991**, *95*, 6073-6075.
37. Wang, J.; Wang, G.; Zhao, J. *Chem. Phys. Lett*. **2003**, *380*(5-6), 716-720.
38. Ono, T.; Hirose, K. *Phys. Rev. Lett*. **2007**, *98*, 026804.
39. Miehlich, B.; Savin, A.; Stoll, H.; Preuss, H. *Chem Phys Lett*. **1989**, *157*, 200-206.